

Full length article

# Crush dynamics and transient deformations of elastic-plastic Miura-ori core sandwich plates



Anup Pydah, R.C. Batra\*

Department of Biomedical Engineering and Mechanics, Virginia Polytechnic Institute and State University, M/C 0219, Blacksburg, VA 24061, USA

## ARTICLE INFO

## Keywords:

Miura-ori core  
Honeycomb core  
Elastic-plastic material  
Transient deformations  
Plastic dissipation  
Blast mitigation  
Crush dynamics

## ABSTRACT

The response of elastic-plastic Miura-ori core sandwich plates to high-intensity dynamic loads is numerically studied using the commercial finite element software ABAQUS/ Explicit. Crushing simulations conducted on the Miura-ori core over a range of loading rates clearly illustrate the dynamic strengthening of the core by inertial effects, particularly at loading rates relevant to blast experiments. Exploratory design studies have been conducted to determine the influence of the unit cell parameters of the Miura-ori pattern on the energy dissipated by the core through plastic deformations, and to compare its performance with that of square honeycomb cores of equal areal density. Material strain rate effects, a material failure criterion and debonding between the core and the facesheets have not been considered. It is found that for low to moderate load intensities, the Miura-ori core consistently outperforms the corresponding honeycomb core in terms of plastic dissipation (by as much as 68%) and facesheet centroidal deflections, and offers a rich design space to tailor its mechanical performance. However, the plastic energy dissipated in the core as a fraction of the total plastic energy dissipated in the structure is nearly the same for the Miura-ori and the honeycomb core sandwich plates of equal core areal density.

## 1. Introduction

Sandwich panels are efficient modular structures with high stiffness-to-weight ratios and can be tailored to meet various design requirements. The sandwich core, which may be either continuous in the form of a metallic or low strength foam, or discrete in the form of a corrugated sheet or square or hexagonal cell honeycombs can dissipate large amounts of energy through plastic compression, transverse shear deformations and bending [1]. Thus, sandwich panels have found prolific use as blast-mitigation structures.

Numerous studies have been conducted on the mechanical response of foam core sandwich beams and plates subjected to either air or underwater blast loads [2–5]. These investigations have detailed the sequential stages in the response of the sandwich structure namely, the fluid-structure interaction during the blast which imparts a uniform velocity to the outer facesheet, followed by core compression and densification and finally, panel stretching and plastic bending. Various regimes of core deformations have been postulated based on the relative velocities of the facesheets. It has been found that sandwich structures have higher shock resistance (in terms of energy dissipation) than corresponding solid plates of equal mass. For cellular core sandwich structures, both homogenized [6,7] and discrete core models

[8–13] have been used to study the blast response of a variety of core geometries. These have indicated the superiority of the honeycomb architecture over other core geometries. By comparing the finite element simulation results with experimental findings, it was determined that the finite element based software ABAQUS/ Explicit accurately simulates the response of sandwich structures to blast loads [14].

The blast effectiveness of honeycomb cores is well established, however, these cores are known to suffer from a moisture accumulation problem wherein the sealed honeycomb cells trap condensed moisture which can severely deteriorate their mechanical performance over time. This has led designers to conduct physical and virtual tests [15,16] on new core architectures [17–20] which also improve the multi-functional capabilities of sandwich structures. The tessellated Miura-ori fold pattern, which is designed using rigid origami principles and exhibits interesting properties such as a wide range of Poisson's ratios and remarkable buckling and load bearing capabilities [21–23] shows tremendous promise to be employed as an alternative to the honeycomb core. However, most current research studies on the mechanics of the Miura-ori pattern derive its material properties under the assumption of *isometric or rigid folding* [24,25] wherein the Miura-ori patterned sheet is permitted to fold freely without any constraints.

\* Corresponding author.

E-mail addresses: [anpydah@vt.edu](mailto:anpydah@vt.edu) (A. Pydah), [rbatra@vt.edu](mailto:rbatra@vt.edu) (R.C. Batra).

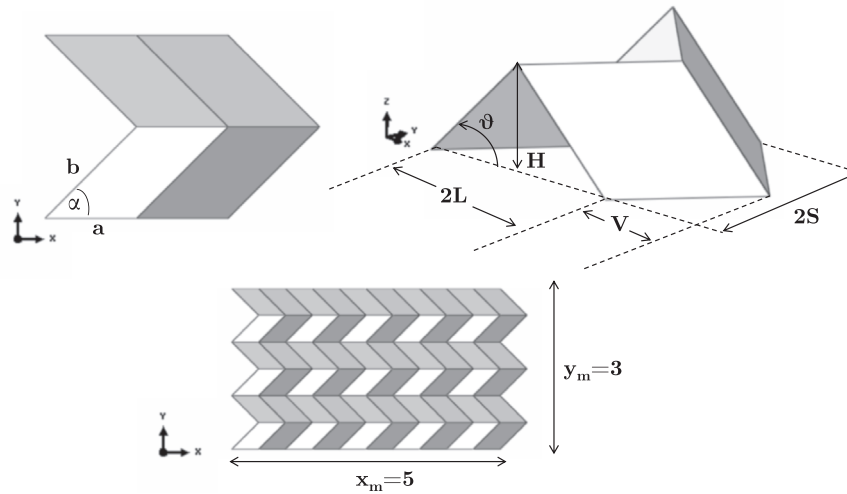


Fig. 1. Geometric parameters of a Miura-ori unit cell.

Thus, the parallelogram facets between the creases remain rigid and deformation is confined only to the fold lines. In such a scenario, the Miura-ori sheet behaves as a mechanism with one degree of freedom. On the other hand, when the Miura-ori pattern is used as a sandwich fold core, it must be suitably bonded to the facesheets which restricts its free-folding kinematics and rigid motion. Quasi-static studies have been conducted on Miura-ori sheets sandwiched between rigid plates [26,27] and have helped provide an insight into the mechanical properties of these folded cores. Recently, a stacked folded core concept was introduced [28] for sandwich beams wherein Miura-ori patterned sheets were stacked to produce cores whose collapse kinematics were governed by a distinctive folding mechanism instead of buckling of core facets. This made the core less sensitive to imperfections whilst offering the versatility to alter the collapse mechanics by changing the core geometry.

In applications where the sandwich core is subjected to blast loads and must absorb large quantities of incident energy, dynamic effects are expected to play a significant role. In particular, the mechanics of deformation of the core under dynamic loads may be significantly different and more complicated than the corresponding quasi-static modes of deformation due to the effects of the inertial resistance of the core as has been shown for honeycomb sandwich plates [7]. Hence, using results from quasi-static studies may underestimate the performance of Miura-ori cores under high-intensity dynamic loads, particularly when sandwiched between deformable facesheets. Clearly, in order to employ the Miura-ori geometry as a blast mitigating core, it is imperative to characterize its dynamic collapse kinematics, and compare its performance with that of the ubiquitous honeycomb core. Using detailed numerical calculations with the commercial finite element software ABAQUS/ Explicit ver. 6.14, this paper seeks to:

1. Investigate the contribution of the inertial resistance of the Miura-ori core to its dynamic strengthening by simulating crushing tests on the core. Material strain rate effects, a failure criterion and debonding between the facesheets and the core have not been considered in these computations.
2. Conduct exploratory design studies to ascertain the influence of unit cell parameters of the Miura-ori pattern on the energy dissipated due to plastic deformations of the core as well as on the facesheet centroidal deflections.
3. Compare the blast performance of the Miura-ori cores with that of square honeycomb cores of equal areal density.

Results of the crushing simulations on the Miura-ori core indicate that the loading strain rate plays an important role in the dynamic

strengthening of the core, particularly for high-intensity impulses relevant to blast loaded sandwich plates. Using the centroidal transient deflections and transverse velocities of the facesheets to characterize the response of the Miura-ori core sandwich plates, the design studies show that the Miura-ori core consistently outperforms corresponding honeycomb cores while offering a rich and versatile design space to tailor its mechanical performance.

The layout of the paper is as follows. The geometry of the Miura-ori core sandwich plate and details of its finite element modeling with ABAQUS/ Explicit are described in Section 2. The effects of inertial hardening on the Miura-ori core during dynamic crushing are investigated in Section 3. The collapse kinematics and the response of the Miura-ori core sandwich plate with deformable facesheets under the action of high-intensity dynamic loads are explained in Section 4. Results from design studies on the influence of unit cell parameters on the response of the Miura-ori core are presented in Section 5, with particular emphasis on plastic dissipation in the core. In Section 6 we have compared the performance of the Miura-ori core with that of honeycomb cores of equal areal density. Conclusions of the work are summarized in Section 7.

## 2. Geometry and modeling of the Miura-ori core sandwich plate

A single Miura-ori unit cell consists of four identical parallelograms and can be characterized by four parameters in its unfolded state: side lengths  $a$  and  $b$ , acute angle  $\alpha$  and the thickness of the sheet material  $t_s$  (Fig. 1). In a particular folded configuration, the Miura-ori unit cell can be completely characterized with one additional parameter: the dihedral fold angle  $\theta$  between the facets and the horizontal base. The unit cell can also be described by its outer dimensions, height  $H$ , width  $2S$ , length  $2L$  and amplitude  $V$  given by ([21])

$$H = a \sin \theta \sin \alpha$$

$$S = b \frac{\cos \theta \tan \alpha}{\sqrt{1 + \cos^2 \theta \tan^2 \alpha}}$$

$$L = a \sqrt{1 - \sin^2 \theta \sin^2 \alpha}$$

and

$$V = b \frac{1}{\sqrt{1 + \cos^2 \theta \tan^2 \alpha}} \tag{1}$$

With the outer dimensions specified, the unit cell parameters can be easily determined ([21]). A planar Miura-ori core consists of  $x_m$  and  $y_m$  unit cells tessellated along and across the corrugation, respectively. The mass density of the Miura-ori core is given by

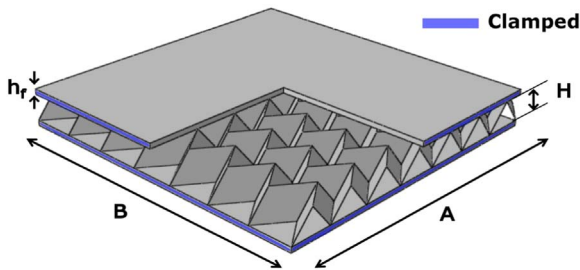


Fig. 2. Miura-ori core sandwich plate.

$$\rho_c = \frac{a b t_s \sin \alpha}{H S L} \rho_m \quad (2)$$

where  $\rho_m$  is the mass density of the core material.

Fig. 2 depicts a Miura-ori core sandwich plate that consists of two identical facesheets of dimensions  $A \times B \times h_f$  while the core thickness is  $H$ . The edges of the facesheets are rigidly clamped and loads are applied to the outer surface of the top facesheet. In order to compare the performance of the Miura-ori core with that of a square honeycomb core of equal areal density, the facesheet dimensions were fixed at  $100 \times 100 \times 2$  mm while a unified core density of approximately  $0.05\rho_m$  was used.

The facesheets of the sandwich plate were meshed using eight-node brick elements with reduced integration and relaxed stiffness hourglass control (element type C3D8R). Each facesheet was discretized with three uniform layers of elements through the thickness and 60 uniform elements along each side. Each parallelogram facet of the Miura-ori core was uniformly meshed with  $20 \times 20$  four-node linear shell elements with reduced integration, hourglass control and finite membrane strains (element type S4R), and the core was attached to the facesheets using the tie constraint which ensures perfect bonding. The ABAQUS general contact algorithm was employed to define frictionless contact between all surfaces.

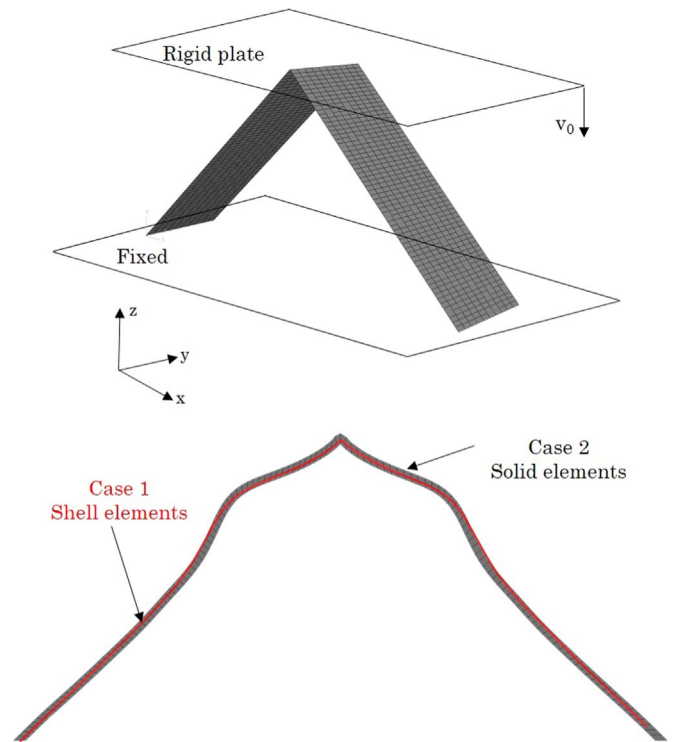
A homogeneous, isotropic, bilinear elastic-plastic material that obeys the von Mises yield criterion with isotropic hardening was selected for both, the facesheets and the Miura-ori core. The material is representative of High Strength Low Alloy steel HSLA-65 with density  $\rho_m = 7800 \text{ kg m}^{-3}$ , Young's modulus  $E = 200 \text{ GPa}$ , Poisson's ratio  $\nu = 0.3$ , yield stress  $\sigma_y = 300 \text{ MPa}$  and the hardening tangent modulus  $E_t = 2 \text{ GPa}$ . With the objective of this work being to conduct exploratory design studies on the blast response of the Miura-ori core sandwich plate, material strain rate effects, a material failure criterion and debonding between the core and facesheets have not been considered.

The capability of the software, ABAQUS/Explicit, and our using it properly was verified by first analyzing the dynamic buckling of a non-linear elastic bar due to a time-dependent load. It was found that the dynamic buckling load increased with an increase in the applied strain-rate that agreed qualitatively with the result reported by Batra and Geng [29]. The quantitative difference is due to different constitutive relations employed in the two studies. ABAQUS/Explicit does not have the St. Venant-Kirchhoff material used in Ref. [29]. Then, simulations were conducted for metallic honeycomb sandwich panels subjected to blast loads used in experiments of Dharmasena et al. [10]. The simulations captured the large deformations in the structure including the buckling of the webs and compared well with experimental measurements.

### 3. Inertial effects during the dynamic crushing of a Miura-ori core

#### 3.1. Results from using shell and 3-D finite elements

Before studying the inertial strengthening of a Miura-ori core under high-intensity, short-duration dynamic loads, we investigate the fidelity of the four-node linear shell elements (element type S4R) by comparing

Fig. 3. Crushing test on a 90 deg fold (deformed shapes at  $\bar{\epsilon} = 0.1$ ).

its performance with that of the three-dimensional eight-node brick elements (element type C3D8R) and its capability of capturing important metrics involved in a blast study including the elastic wave speed within the core as well as the crushing and buckling deformation patterns observed in the facets of the core. Consider a 90 deg fold of thickness  $0.35 \text{ mm}$  sandwiched between two rigid plates  $H = 10 \text{ mm}$  apart, as shown in Fig. 3, and very long in the  $y$  direction (plane strain conditions). The top facesheet is suddenly moved downwards with a velocity  $V_0 = 10 \text{ m/s}$ , while the bottom facesheet is fixed rigidly, which mimics a blast loading scenario. In order to yield converged results, for the first case, each web of the fold was uniformly meshed with 60 shell elements along its length while for the second case, each web was uniformly meshed with 60 solid elements along its length and 4 uniform layers of elements through its thickness. For the material considered in this study, the 1-dimensional elastic and plastic wave speeds in a homogeneous solid plate can be calculated as  $c_0 = \sqrt{E/\rho} = 5.06 \text{ mm}/\mu\text{s}$  and  $c_p \approx \sqrt{E_t/\rho} = 0.51 \text{ mm}/\mu\text{s}$ , respectively. The time taken by the elastic wave to travel through the fold and reach the bottom facesheet is estimated to be  $2.80 \mu\text{s}$ . For both cases, the time taken for the elastic wave to reach the middle and bottom of the web were determined by studying the time variation of compressive stresses in elements at those locations, and were calculated as  $1.45 \mu\text{s}$  and  $2.77 \mu\text{s}$ , respectively. Furthermore, at an overall (engineering) strain  $\bar{\epsilon} \equiv V_0 t/H = 0.1$ , the buckled shape of the web and the specific location of the localized buckling fold were accurately predicted by the shell model, when compared with the results from the 3D model, as shown in Fig. 3. The maximum equivalent plastic strain in the cores as calculated by the shell and 3D models were  $0.105$  and  $0.107$ , respectively. Clearly, the S4R shell elements possess the requisite accuracy to model high-intensity dynamic studies on foldcore sandwich plates.

#### 3.2. Effect of loading rate on crushing deformations

Next we consider a Miura-ori core sandwiched between two rigid plates  $10 \text{ mm}$  apart, as shown in Fig. 4, undergoing a similar crushing test as described earlier. For  $V_0 = 100 \text{ m/s}$ , one measure of the engineering strain rate in the core is  $\bar{\epsilon} \equiv V_0 t/H = 10^4/\text{s}$ . The inertia forces

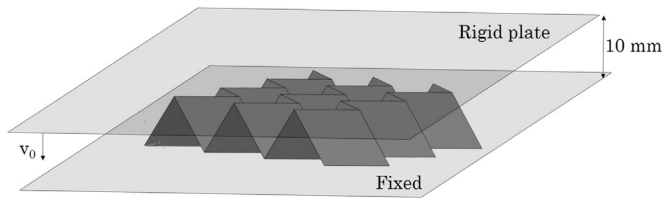


Fig. 4. Crushing test on the Miura-ori core.

developed in the core by its rapid acceleration can help strengthen the core facets. As a result, the core exerts a greater reaction force on the facesheets and can absorb more energy than it would under quasi-static loading. In order to investigate the role of dynamic effects on the deformations in the core, the crushing simulations are conducted on a 3 × 3 grid of Miura-ori unit cells each with dimensions  $a = b = 12.29$  mm,  $\alpha = 61.77$  deg,  $t_s = 0.192$  mm and at a range of overall strain rates varying from  $\dot{\epsilon} = 50$ /s to  $\dot{\epsilon} = 6000$ /s. The area of the core projected onto the facesheets  $A_c = 1838.74$  mm<sup>2</sup>. Each parallelogram facet of the Miura-ori core was uniformly meshed with 20 × 20 S4R shell elements which yielded converged results.

The time variation of the average compressive stress,  $\bar{\sigma} \equiv F_r/A_c$ , where  $F_r$  is the average reaction force exerted on the facesheets by the core, with respect to the engineering strain  $\bar{\epsilon}$  is plotted in Fig. 5 for a range of imposed overall loading strain rates. The large difference between the stresses on the top and the bottom facesheets is because of the inertial effects in the core. Furthermore, there is significant strengthening of the core at high loading strain rates, with peak stress on the top facesheet for the  $\dot{\epsilon} = 6000$ /s case being almost three times as large as that for  $\dot{\epsilon} = 50$ /s. The elastic stress wave reaching the bottom

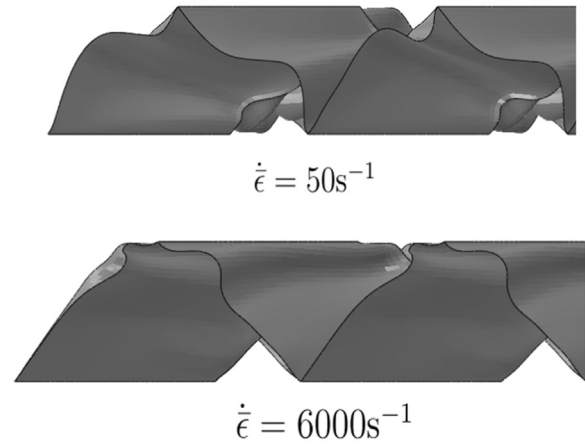


Fig. 6. Side view of the deformed configurations of the core at  $\dot{\epsilon} = 0.3$  for  $\dot{\epsilon} = 50$ /s and  $\dot{\epsilon} = 6,000$ /s.

rigid facesheet causes a small initial stress increase in the bottom facesheet. Before the plastic wave reaches the bottom facesheet, the stress in it remains compressive followed by a steep increase to a value which is approximately twice that experienced by the top facesheet at that instant; this causes the facets of the Miura-ori core to buckle and fold into each other resulting in a loss of stiffness of the core and a sharp drop in the stresses in both facesheets. Once the facets of the core come into contact, densification occurs which causes an increase in the compressive stress on both facesheets.

Side views of the deformed configurations of the core at  $\dot{\epsilon} = 0.3$  for

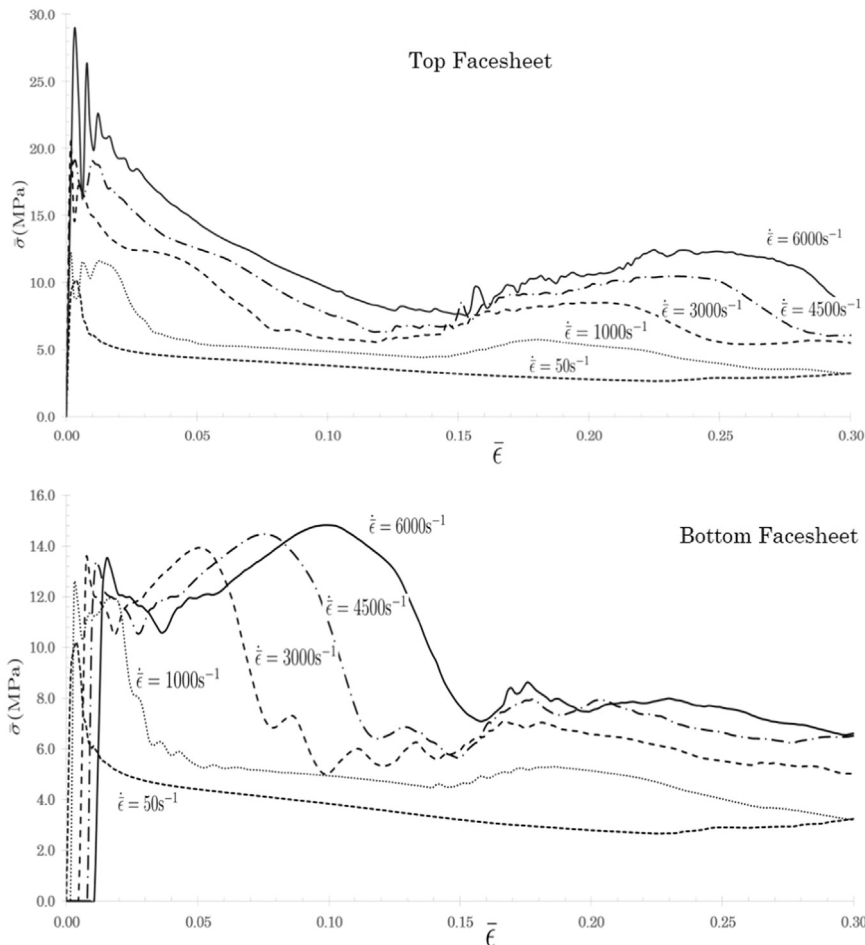


Fig. 5. Average compressive stresses on the top and the bottom facesheets for a range of overall loading strain rates.

both, the low loading strain rate ( $\dot{\epsilon} = 50/s$ ) and the high loading rate ( $\dot{\epsilon} = 6000/s$ ) are depicted in Fig. 6. These clearly indicate that the collapse kinematics of the core are significantly different for the two loading rates. The buckling deformations tend to be localized near the top facesheet for the high-velocity loading, as is expected with the top facesheet experiencing higher compressive stresses, while significant folding and a smooth buckled profile are observed for the low velocity loading. Furthermore, the substantial increase in the compressive stresses on the two facesheets for the higher velocity cases indicate that these cores may be able to absorb large quantities of energy through plastic deformations which makes them attractive blast-mitigating alternatives to the honeycomb core. Clearly, results from quasi-static tests cannot be used to accurately design Miura-ori core sandwich plates for high-intensity dynamic loads.

#### 4. Dynamic response of a Miura-ori core sandwich plate

The collapse kinematics and the response of the Miura-ori core sandwich plate with deformable facesheets under the action of high-intensity dynamic loads are investigated in this section. The dynamic load due to an air blast is modeled as a time-dependent non-uniformly distributed pressure field acting on the outer surface of the top facesheet that exponentially decays with distance  $d$  from the centroid of the top facesheet according to Eq. (3) which is adapted from [10]. The exponential decay of the pressure with the distance  $d$  postulated here is different from that used by Batra and Hassan [30, 33] who derived the spatial variation by fitting a smooth polynomial in  $d$  to the test data of Turkmen and Mecitoglu [31]. A possibility is to assign the same initial velocity to all points of the structure, e.g., see [34]. However, it is not easy to find the value of the initial velocity that will deform the structure essentially the same as the pressure distribution. The peak blast overpressure  $P_0$  is assumed to occur at  $d=0$  and decreases exponentially as given below

$$p(d, t) = \begin{cases} 0 & t < t_a \\ p(t)e^{-(d/d_0)^2} & t_a \leq t \leq t_a + t_d \end{cases} \quad (3)$$

where

$$p(t) = P_0 \left[ 1 - \frac{t - t_a}{t_d} \right] e^{-(t-t_a)/t_d}$$

Here,  $d_0 = 50$  mm is a reference distance,  $t_a = 0.02$  ms is the arrival time,  $t_d = 0.18$  ms is the time duration and  $t_0 = 0.1898$  ms is the decay constant.

We conducted a convergence study on the response of the Miura-ori core sandwich plate with  $\{x_m, y_m\} = \{5, 5\}$ ,  $H = 10$  mm and mesh densities ranging from  $10 \times 10$  elements to  $25 \times 25$  elements in each facet of the Miura-ori core. A blast load given by Eq. (3) with  $P_0 = 100$  MPa is applied to the outer surface of the top facesheet. For the facesheets, 60 uniform elements along each side with three uniform elements through the thickness were found to yield converged results for each case. Key results are presented in Table 1 at  $t = 3$  ms and indicate that the global response quantities like the plastic dissipation in the core and the maximum equivalent plastic strain in the core,  $\epsilon_p$ , as

**Table 1**  
Mesh convergence study for the Miura-ori core with  $\{x_m, y_m\} = \{5, 5\}$  and  $H = 10$  mm at  $t = 3$  ms.

Miura-ori facet mesh density	PD core (kJ)	$\epsilon_p$	Deflection (mm)	
			Bottom	Top
10 × 10	0.394	0.782	15.13	19.72
15 × 15	0.423	0.987	14.84	19.50
20 × 20	0.427	1.108	14.93	19.68
25 × 25	0.427	1.112	14.94	19.68

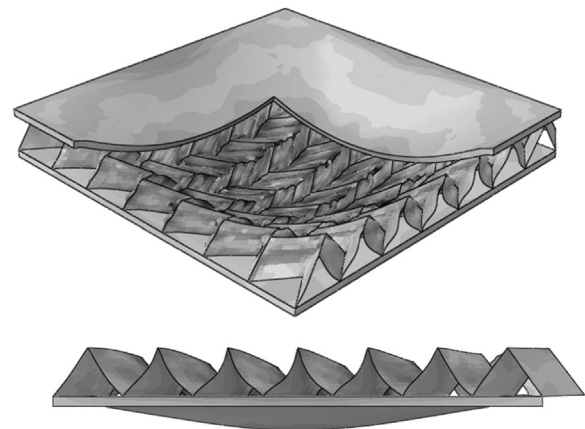


Fig. 7. Deformed shape of the Miura-ori core sandwich plate.

well as local quantities like the facesheet centroidal deflections, converged for the  $20 \times 20$  FE mesh in each facet of the Miura-ori core. The number of shell elements in the core models used in this study range from 14,400 to 78,400.

Fig. 7 shows the computed deformed shape at  $t = 3$  ms of the sandwich panel corresponding to  $\{x_m, y_m\} = \{7, 7\}$  with  $a = b = 12.29$  mm,  $\alpha = 61.77$  deg,  $t_s = 0.192$  mm and  $H = 10$  mm. The facesheet dimensions are  $100 \times 100 \times 2$  mm and the edges are rigidly clamped. A blast load given by Eq. (3) with  $P_0 = 100$  MPa is applied to the outer surface of the top facesheet. At the center of the core, the primary deformation mode is the folding and densification of the facets while near the edges, away from the blast load peak, the facets tend to bend inwards reducing the distance between the facets. This response is depicted in detail in Fig. 8 where attention is focused on the four Miura-ori unit cells situated at the center of the core using two different viewing angles. As compression of the core progresses, the mountain folds on the top of the unit cells are flattened followed by folding and densification of the facets which come into contact with the facesheets. The computed work done by the applied pressure field at  $t = 3$  ms was 1.94 kJ while the sum of the kinetic energy (0.2 J), the elastic strain energy (9.2 J) and the plastic dissipation (1.85 kJ) was determined as 1.86 kJ. Thus the energy dissipated due to the hour glass modes that could ensue because of the reduce integration was 4.1% of the work done by the applied pressure.

The time histories of the vertical displacements and velocities of the centroidal node at the bottom of each facesheet, as well as the *centroidal core compression*, defined as the difference between the centroidal deflections of the bottom surface of the top facesheet and the top surface of the bottom facesheet are shown in Fig. 9. Fig. 10 shows the time evolution of the energy dissipated through plastic deformations in each of the three components of the sandwich plate. Fig. 11 depicts the time histories of the total kinetic energy, total strain energy and plastic dissipation in the sandwich plate, as well as the work done by the blast load on the structure. Three phases of response, similar to those for foam core sandwich plates [2], are observed.

1. Centroidal core compression ( $0 < t < 0.12$  ms): The top facesheet begins to accelerate faster than the bottom facesheet because of the time taken by the loading wave to arrive at the bottom facesheet causing the height of the center of the core to reduce (and the centroidal core compression to increase). Significant plastic deformations in the core help to restrict the kinetic energy imparted by the blast (see Figs. 10 and 11) in this phase. As the core transfers momentum to the bottom facesheet, its velocity increases while the top facesheet begins to decelerate. This phase ends with the equalization of velocities of both facesheets and the centroidal core compression reaches its maximum value.
2. Panel bending and stretching ( $0.12 < t < 0.21$  ms): Both facesheets

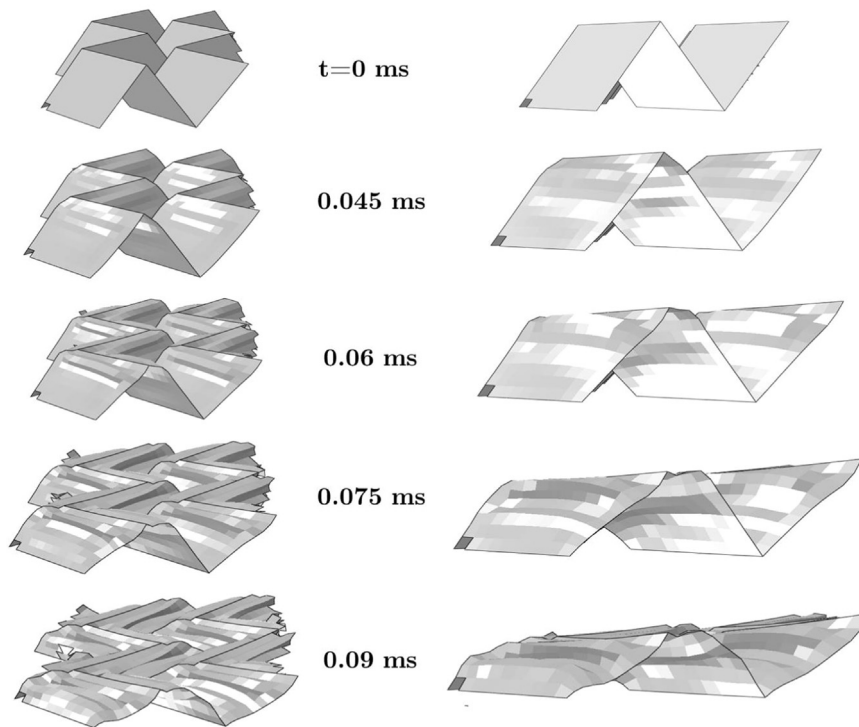


Fig. 8. Deformed shapes of centrally situated Miura-ori unit cells at various times.

move together as the sandwich plate plastically bends with minimal change in the centroidal core compression. With the edges of the facesheets clamped, there is an increase in the plastic dissipation in the facesheets due to bending and stretching (see Fig. 10). This helps to significantly dissipate the kinetic energy in the structure (see

Fig. 11) and reduce speeds of the facesheets which reach their points of maximum centroidal deflection at the end of this stage. Minimal additional plastic deformations occur in the core and the magnitude of the centroidal core compression at the end of phase I dictates the sandwich plate bending stiffness in this phase.

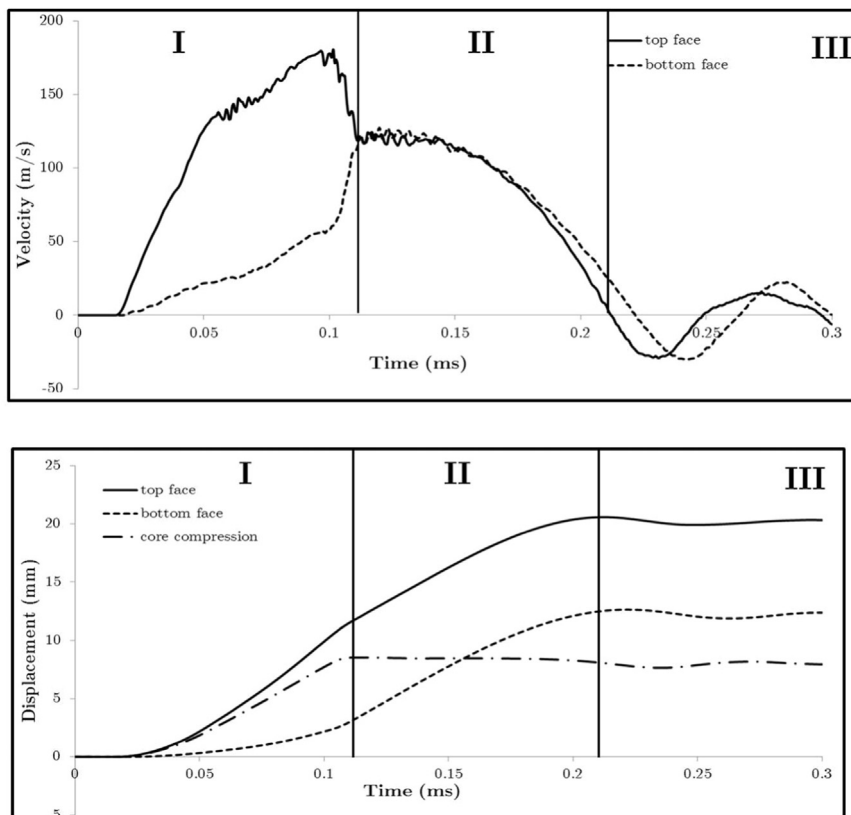


Fig. 9. Time evolution of centroidal velocities and displacements of the facesheets.

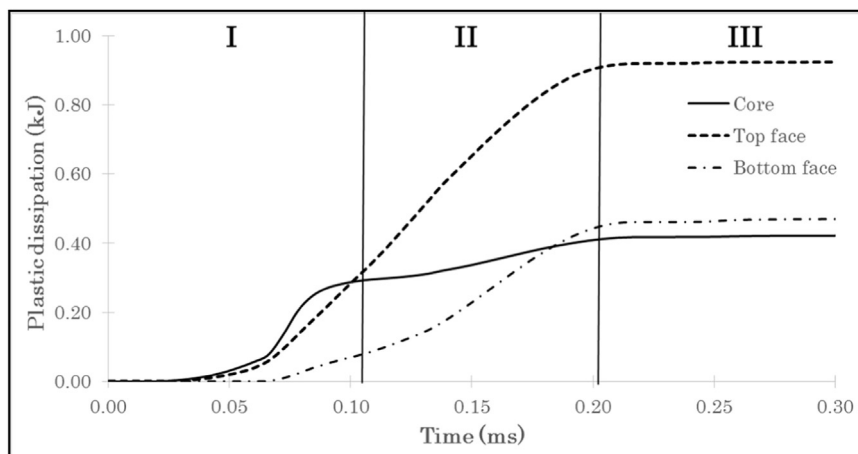


Fig. 10. Time evolution of plastic dissipation in the facesheets and the core.

3. Elastic oscillations about the final deflected state ensue which then die out at approximately 3 ms (not shown in the figure) due to structural plastic deformations.

From Figs. 9, 10 and 11, it is clear that a significant fraction of the total energy is dissipated through plastic compression of the core, particularly in the first phase of the response. This observation has motivated us to study the influence of the unit cell parameters of the Miura-ori pattern on the plastic dissipation in the core and compare its performance with that of square honeycomb cores of equal areal density.

**5. Influence of unit cell parameters on plastic dissipation of the Miura-ori core**

Recall that a Miura-ori unit cell is characterized by four parameters—the side lengths  $a$  and  $b$ , the acute angle  $\alpha$  and the thickness of the sheet material  $t_s$ . These provide a diverse design space to help tailor the blast resistance of the Miura-ori core for maximum energy dissipated due to plastic deformations. We restrict ourselves to rhombic unit cells ( $a = b$ ) and fix the overall core dimensions to  $100 \times 100 \times 5$  mm. By choosing appropriate values of the number of unit cells  $\{x_m, y_m\}$ , the side length  $a$  and angle  $\alpha$  can be varied (see Eqs. (1)); increasing the number of unit cells along the corrugation ( $x_m$ ) reduces the side length  $a$  while increasing the number of cells across the corrugation ( $y_m$ ) reduces the acute angle  $\alpha$ . It should be noted that once  $x_m$ , and hence  $a$  is chosen,  $y_m$  is restricted to be greater than or equal to  $x_m$ . The final parameter, the thickness  $t_s$  of the sheet material is adjusted to maintain the relative core density at 0.05 (Eq. (2)). In Table 2 we have summarized the 15

**Table 2**  
Unit cell geometries of the Miura-ori core models.

Case	$x_m$	$y_m$	$a$ (mm)	$\alpha$ (degrees)	$\theta$ (degrees)	$t_s$ (mm)
1	3	3	17.401	74.03	17.39	0.239
2	3	4	17.401	48.22	22.67	0.231
3	3	5	17.401	38.39	27.57	0.222
4	3	6	17.401	32.77	32.06	0.212
5	3	7	17.401	29.14	36.16	0.202
6	4	4	13.463	69.83	23.31	0.230
7	4	5	13.463	51.56	28.30	0.220
8	4	6	13.463	43.18	32.87	0.210
9	4	7	13.463	38.09	37.01	0.200
10	5	5	11.180	66.42	29.21	0.218
11	5	6	11.180	53.40	33.85	0.208
12	5	7	11.180	46.52	38.05	0.197
13	6	6	9.718	63.82	34.98	0.205
14	6	7	9.718	54.45	39.23	0.194
15	7	7	8.719	61.98	40.51	0.190

unit cell geometries chosen by increasing  $x_m = y_m$  by 1 for the design study. Blast loads given by Eq. (3) with  $P_0 = 100$  MPa and 300 MPa are applied to the outer surface of the top facesheet of each sandwich plate.

Based on the finite element simulations carried out till  $t = 3$  ms, we have summarized in Table 3 the total plastic energy dissipated (in kJ) by the Miura-ori cores, along with the plastic dissipation in the core as fractions of the work done on the plate and the total energy dissipation in the entire sandwich structure. In Table 4 we have listed the top and the bottom facesheet centroidal deflections. Based on these results, the following observations are made:

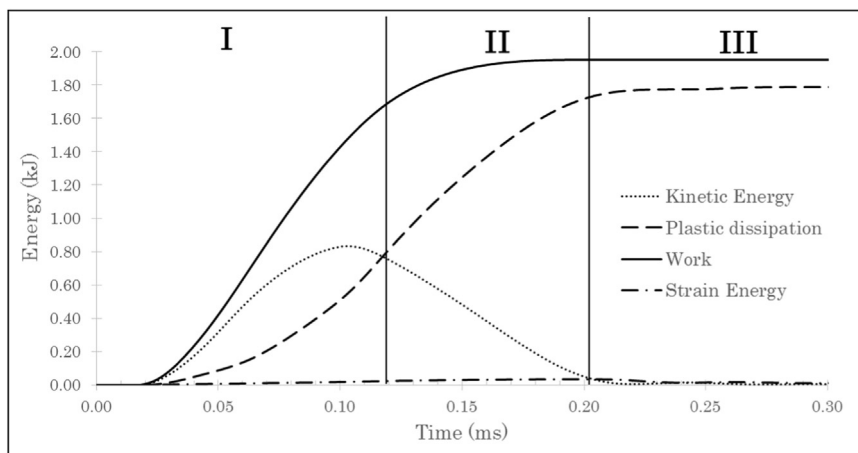


Fig. 11. Time histories of the total kinetic energy, total strain energy and plastic dissipation in the sandwich plate and work done by the blast load.

**Table 3**  
Plastic dissipation in the Miura-ori cores for  $P_0 = 100$  MPa and (300 MPa).

$x_m \rightarrow$		Plastic dissipation in the core (kJ)									
$y_m \downarrow$		3		4		5		6		7	
3		0.188	(0.949)								
4		0.276	(1.222)	0.302	(1.300)						
5		0.346	(1.470)	0.371	(1.530)	0.427	(1.563)				
6		0.416	(1.697)	0.443	(1.782)	0.467	(1.855)	0.485	(1.879)		
7		0.463	(1.791)	0.500	(1.974)	0.520	(2.052)	0.535	(2.114)	0.547	(2.193)

$x_m \rightarrow$		PD <sup>a</sup> core/Total PD									
$y_m \downarrow$		3		4		5		6		7	
3		0.11	(0.07)								
4		0.15	(0.08)	0.17	(0.09)						
5		0.19	(0.10)	0.21	(0.11)	0.22	(0.11)				
6		0.23	(0.12)	0.24	(0.12)	0.26	(0.13)	0.27	(0.13)		
7		0.26	(0.12)	0.27	(0.13)	0.28	(0.14)	0.29	(0.14)	0.30	(0.15)

$x_m \rightarrow$		PD core/Work									
$y_m \downarrow$		3		4		5		6		7	
3		0.09	(0.06)								
4		0.14	(0.08)	0.15	(0.08)						
5		0.17	(0.09)	0.19	(0.10)	0.20	(0.10)				
6		0.21	(0.11)	0.22	(0.11)	0.24	(0.12)	0.25	(0.12)		
7		0.23	(0.12)	0.25	(0.13)	0.26	(0.13)	0.27	(0.14)	0.28	(0.14)

<sup>a</sup> PD = Plastic dissipation.

1. Increasing the number of unit cells along the corrugation ( $x_m$ ) or equivalently, decreasing the side length  $a$  by a factor of 2 dramatically increases the energy dissipated by the core through plastic deformations by a factor of 3 for  $P_0 = 100$  MPa. Furthermore, as a function of the total energy dissipated in the structure, the core contributions increase significantly, from 11% to 30%; this can also be viewed as an increase in the “efficiency” of the core (with regards to plastic dissipation).
2. Similar trends are observed when decreasing the angle  $\alpha$  between the sides of a unit cell (this is equivalent to increasing the number of unit cells across the corrugation ( $y_m$ )) - the plastic energy dissipated by the core and its efficiency increase by 18% and 15% respectively.
3. For the higher blast intensity ( $P_0 = 300$  MPa), the same observations hold. However, the core efficiency and the fraction of total work dissipated through plastic deformations of the core are lower than

those for  $P_0 = 100$  MPa by a factor of 2.

4. The facesheet centroidal deflections are essentially unaffected by changing the unit cell parameters. Decreasing the side length  $a$  seems to marginally reduce the bottom facesheet centroidal deflection for  $P_0 = 100$  MPa, while having negligible influence on the top facesheet centroidal deflections. For  $P_0 = 300$  MPa, the top face deflections actually increase with an increase in the number of unit cells. This agrees with the previous observation- a higher top facesheet centroidal deflection due to a higher intensity load would result in an increase in the plastic dissipation in the top facesheet thereby reducing the core efficiency. Further, this would also result in a greater amount of work done by the blast load on the structure and hence reduce the fraction of the work dissipated by the core through plastic deformations.

**Table 4**  
Facesheet centroidal deflections for the Miura-ori cores for  $P_0 = 100$  MPa and (300 MPa).

$x_m \rightarrow$		Bottom facesheet deflection (mm)									
$y_m \downarrow$		3		4		5		6		7	
3		15.17	(39.61)								
4		15.21	(39.94)	14.97	(40.06)						
5		15.29	(40.60)	15.08	(40.76)	14.93	(40.79)				
6		15.47	(40.65)	15.00	(40.66)	14.91	(40.86)	14.70	(40.84)		
7		14.86	(40.08)	14.81	(40.84)	14.87	(40.88)	14.93	(40.93)	14.81	(40.81)

$x_m \rightarrow$		Top facesheet deflection (mm)									
$y_m \downarrow$		3		4		5		6		7	
3		19.66	(44.79)								
4		19.67	(45.20)	19.70	(45.19)						
5		19.55	(45.71)	19.67	(45.92)	19.68	(45.99)				
6		19.49	(45.86)	19.54	(45.90)	19.59	(46.01)	19.67	(46.05)		
7		19.55	(45.39)	19.68	(46.05)	19.54	(46.06)	19.43	(46.16)	19.50	(46.15)

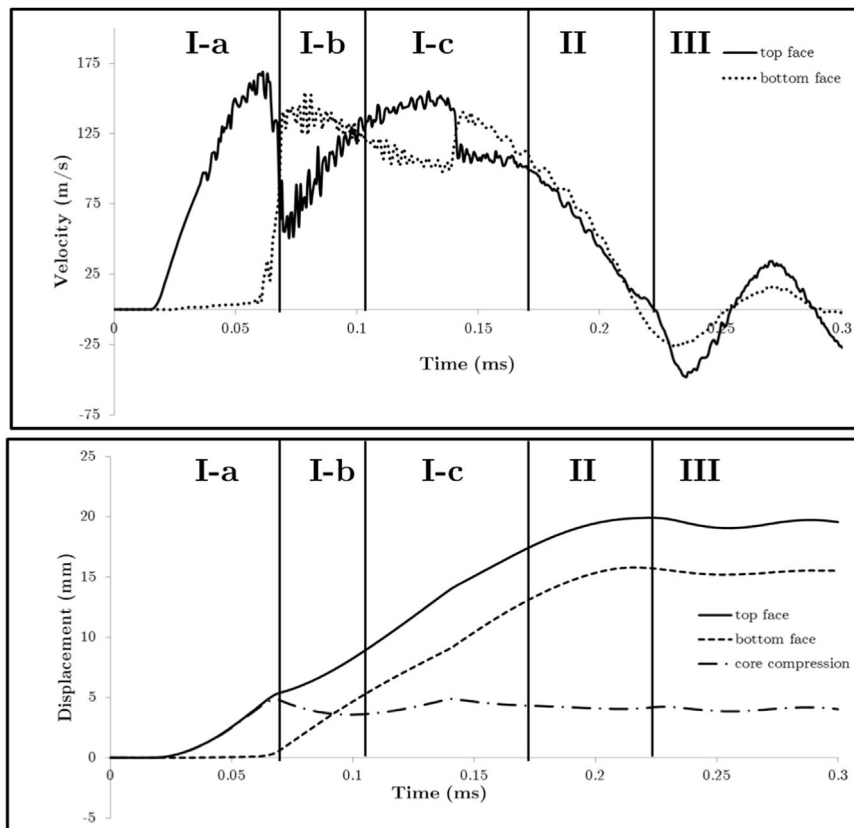


Fig. 12. Time evolution of centroidal velocities and displacements of the facesheets for  $\{x_m, y_m\} = \{3, 6\}$ .

With regard to core compression, a non-monotonic trend is observed- depending upon the side length  $a$ , reducing the angle  $\alpha$  can cause an increase or decrease of the core compression, switching between a “soft” and “hard” core response. Such a trend is to be expected- the geometry of the core and the thickness of the core sheet affect the core compliance, so, changing the unit cell geometry or increasing the number of unit cells requires a change in the thickness of the core sheet (to maintain its constant areal density) that can cause a non-monotonic change in the stiffness of the core against compression; this indicates the need to tailor the unit cell parameters carefully.

In order to demonstrate the effect of the core design on its response, results are presented for a Miura-ori core sandwich plate with  $\{x_m, y_m\} = \{3, 6\}$ ; this corresponds to Case 4 in Table 2. Fig. 12 shows time histories of the displacements and velocities of the centroidal node at the bottom of each facesheet along with the centroidal core compression. On comparing the results with those depicted in Fig. 9, a number of different features can be noted with regard to the centroidal core compression phase of the response, which is now divided into three sub-regimes:

1. Core densification: The bottom facesheet remains stationary as the top facesheet accelerates towards it while compressing the core. Upon complete densification of the core (when the height of the core reduces to  $\sim 0$  mm), the top facesheet “slaps” [5] against the bottom facesheet transferring a part of its momentum to the bottom facesheet and resulting in a drop of the top facesheet velocity.
2. Core recovery: As a result of the faceslap, there is a sudden increase in the bottom facesheet velocity and it displaces away from the top facesheet causing the core to “spring back”, partly reducing the core compression.
3. Velocity equalization: As the core regains a part of its stiffness due to the spring back, it pulls the facesheets together in an attempt to equalize their velocities. For this particular Miura-ori core geometry

and intensity of loading, the core does not have sufficient stiffness to prevent a second faceslap due to complete densification. This process of momentum transfer between the facesheets continues till their velocities equalize.

In the first phase of the response to a blast load, the primary function of the core is to reduce the top facesheet velocity through a combination of plastic core compression and transfer of momentum to the bottom facesheet. A stiff core would suffer less compression but would transfer a large fraction of its momentum to the bottom facesheet resulting in severe permanent deflection which could be dangerous to the payload/ occupants that the structure is designed to protect. On the other hand, a highly compliant core might be able to significantly dissipate the kinetic energy of the top facesheet through plastic deformations, but it may not possess the requisite compressive strength to prevent complete densification. This could result in multiple faceslaps, each giving rise to large support reactions and a much lower overall stiffness of the sandwich structure as it moves to the next phase of the response- panel bending. These conflicting requirements indicate that the ability to tailor the mechanical characteristics of the core is particularly important to optimize structural performance. The studies presented above clearly demonstrate the versatility and the rich design space offered by the Miura-ori core. Furthermore, by adjusting a few geometric parameters, a wide range of response characteristics can be achieved to help mitigate different blast threats.

### 5.1. Limitations of the current analysis

Material strain-rate and thermal-softening effects, debonding between the facesheets and the core, as well as damage initiation and propagation in the structural components have not been considered. Furthermore, no imperfections are introduced in the design of Miura-ori core.

**Table 5**  
Unit cell geometries of the square honeycomb cores.

Case	$x_m$	$y_m$	$t_s$ (mm)
1	3	3	0.833
2	4	4	0.625
3	5	5	0.500
4	6	6	0.417
5	7	7	0.357

**Table 6**  
Unit cell geometries of the Miura-ori and the honeycomb cores for  $H = 10$  mm.

Case	$x_m$	$y_m$	Miura-ori unit cell				Honeycomb	
			$a$ (mm)	$\alpha$ (degrees)	$\theta$ (degrees)	$t_s$ (mm)	$t_s$ (mm)	
1	3	3	19.437	63.82	34.98	0.410	0.833	
2	5	5	14.142	60.00	54.74	0.289	0.500	
3	7	7	12.289	61.77	67.45	0.192	0.357	

**6. Comparison with honeycomb cores of equal areal density**

The square honeycomb architecture has been shown to be effective for blast-resistant structures. Square honeycomb cores of equal areal density and overall dimensions as that of the Miura-ori cores ( $100 \times 100 \times 5$  mm) are chosen for the comparative study; attention is restricted to cores with an equal number of webs in both directions, also denoted by  $\{x_m, y_m\}$ .

In Table 5 we have listed the 5 honeycomb geometries chosen for the study; the thickness  $t_s$  of the webs is adjusted to maintain a relative core density of 0.05. Blast loads given by Eq. (3) with  $P_0 = 100$  MPa and 300 MPa are applied to the outer surface of the top facesheet of each honeycomb sandwich plate. In Table 7 we have summarized the total plastic energy dissipated in kJ by the honeycomb cores, along with the plastic dissipation in the core as fractions of the work done on the plate and the total plastic energy dissipation in the entire sandwich structure. Also listed are the top and the bottom facesheet centroidal deflections. On comparison with the response of the Miura-ori cores presented in Tables 3 and 4, the following key observations are made:

1. In terms of plastic energy dissipated by the cores and the core efficiency (defined as the energy dissipated by the core as a fraction of the total plastic dissipation by the structure), the Miura-ori cores consistently outperform the square honeycomb cores for both load intensities. With  $\{x_m, y_m\} = \{7, 7\}$  for both cores, the Miura-ori core dissipates 123% more energy through plastic deformations and has 66% greater core efficiency than the honeycomb core for  $P_0 = 100$  MPa. For  $P_0 = 300$  MPa, the Miura-ori core dissipates 7% more energy through plastic deformations. The performance of the honeycomb core improves at higher loads because a greater fraction of the webs buckle plastically which increases the energy dissipation by the core and the top facesheet centroidal deflections. This indicates that while the Miura-ori cores consistently show better performance than the honeycomb cores of the same areal density, they are particularly effective at the lower blast intensity.

**Table 7**  
Plastic dissipation and facesheet centroidal deflections of the honeycomb cores for  $P_0 = 100$  MPa and (300 MPa).

Case	PD core	(kJ)	PD core/Total PD	PD core/Work	Bottom facesheet deflection (mm)		Top facesheet deflection (mm)	
1	0.196	(1.280)	0.14(0.09)	0.14(0.09)	15.90	(40.09)	16.64	(42.94)
2	0.223	(1.733)	0.16(0.12)	0.16(0.12)	15.54	(40.00)	17.36	(44.36)
3	0.229	(1.792)	0.17(0.12)	0.16(0.13)	15.72	(40.60)	16.82	(43.92)
4	0.250	(2.070)	0.19(0.14)	0.18(0.14)	15.41	(40.11)	17.15	(45.36)
5	0.245	(2.054)	0.18(0.14)	0.17(0.14)	15.51	(40.51)	16.77	(44.26)

2. For  $P_0 = 100$  MPa, the bottom facesheet centroidal deflections of the Miura-ori core sandwich plates are less than those of the honeycomb sandwich plates indicating the greater structural integrity offered by the Miura-ori core. For  $P_0 = 300$  MPa, the bottom facesheet centroidal deflections are similar for both cores.
3. An important feature of these results is that in comparison with the honeycomb core, the Miura-ori core offers a wide range of response capabilities (in terms of the plastic dissipation and the core efficiency) that can be achieved by tuning a few geometric parameters of the core.

In order to ascertain the importance of the core height  $H$ , we now analyze deformations of sandwich plates having  $H = 10$  mm with the dimensions of the facesheets unchanged. In Table 6 we have listed the geometries of the 3 Miura-ori and the 3 honeycomb cores chosen. In Table 8 we have summarized the total plastic energy dissipated by the core, the core efficiency, and facesheet centroidal deflections for the two core architectures. Similar qualitative trends are observed as before- the Miura-ori core consistently dissipates more energy through plastic deformations with a higher core efficiency than the honeycomb core, while the Miura-ori core sandwich plate undergoes less bottom facesheet centroidal deflections than the honeycomb sandwich plate.

Table 9 summarizes the effects of the blast loading intensity ( $P_0$  in Eq. (3)) on the plastic dissipation in the core, the core efficiency and the bottom facesheet centroidal deflections of the Miura-ori and the honeycomb cores. The geometry chosen for the two core architectures corresponds to Case 3 of Table 6 with  $\{x_m, y_m\} = \{7, 7\}$ . Irrespective of the loading intensity, the energy dissipated by the Miura-ori core is larger than that by the honeycomb core. This is particularly evident for lower load intensities (for  $P_0 < 200$  MPa), where the Miura-ori core dissipates on average, 23% or greater energy than the honeycomb core. As the load intensity increases, a greater fraction of the honeycomb webs buckle plastically, thereby increasing the energy dissipated within the honeycomb core. However, the bottom facesheet centroidal deflections of the Miura-ori sandwich plate are always less than that of the honeycomb sandwich plate. It should be noted that for loads till  $P_0 = 200$  MPa, the maximum principal plastic strain in the Miura-ori cores is less than the failure strain  $\epsilon_f = 0.5$  ([32]) for the material considered (at  $P_0 = 200$  MPa, the maximum principal plastic strain in the core is 0.496). However, the maximum principal plastic strain in the core for  $P_0 = 300$  MPa exceeds the failure strain, indicating that these cores are suitable for lower load intensities ( $P_0 \leq 200$  MPa).

To predict which component of the sandwich structure (i.e., facesheets or core) would fail first, we have listed in the second and the third column of Table 10 the maximum equivalent plastic strain induced in each facesheet and the core for the Miura-ori and the honeycomb core geometries detailed in Table 6 for  $P_0 = 100$  MPa. Consistent with our earlier observation that the Miura-ori core dissipates significantly more energy through plastic deformations than the honeycomb core, we see that the maximum plastic strain in the Miura-ori core is larger than that in the corresponding honeycomb core. This indicates that a Miura-ori core may fail at a lower value of  $P_0$  than a honeycomb core of equal areal density. However, the maximum plastic strain induced in the bottom facesheets is lower for the Miura-ori core sandwich plates as compared to the honeycomb sandwich plates indicating the greater structural integrity of the Miura-ori core sand-

**Table 8**

Plastic dissipation and facesheet centroidal deflections of the Miura-ori and the honeycomb cores for  $H = 10$  mm and  $P_0 = 100$  MPa and (300 MPa).

Case	PD core (kJ)		PD core/Total PD		PD core/Work		Bottom facesheet deflection (mm)		Top facesheet deflection (mm)	
	Miura	HC <sup>a</sup>	Miura	HC	Miura	HC	Miura	HC	Miura	HC
1	0.538 (2.124)	0.352 (2.666)	0.26 (0.14)	0.27 (0.19)	0.24 (0.13)	0.26 (0.18)	11.57 (33.59)	13.47 (35.50)	20.57 (43.01)	14.37 (40.31)
2	0.657 (3.922)	0.390 (3.315)	0.35 (0.25)	0.31 (0.22)	0.32 (0.24)	0.29 (0.22)	11.95 (35.01)	13.29 (36.21)	20.09 (45.12)	14.87 (42.93)
3	0.603 (3.952)	0.402 (3.684)	0.33 (0.25)	0.31 (0.25)	0.31 (0.24)	0.30 (0.23)	12.07 (35.38)	13.26 (36.16)	20.15 (45.34)	15.03 (42.80)

<sup>a</sup> HC=Honeycomb core.

**Table 9**

Effects of loading intensity on the blast performance of Miura-ori and honeycomb sandwich plates.

$P_0$ (MPa)	PD core (kJ)		PD core/Total PD		Bottom facesheet deflection (mm)	
	Miura	HC	Miura	HC	Miura	HC
50	0.147	0.122	0.42	0.48	5.82	5.74
100	0.603	0.402	0.33	0.31	12.08	13.26
200	2.039	1.648	0.28	0.27	24.83	25.73
300	3.952	3.684	0.25	0.25	35.38	36.16
400	6.484	5.953	0.24	0.22	46.47	46.59

**Table 10**

Maximum plastic strain, strain rate and local temperature rise in the Miura-ori and the honeycomb core sandwich plates for  $H = 10$  mm.

	$\epsilon_p$		$\dot{\epsilon}_p$ ( $s^{-1}$ )		$\Delta T_r$ (K)	
	Miura	HC	Miura	HC	Miura	HC
<b>Case 1 {3, 3}</b>						
Top facesheet	0.400	0.225	2667	500	62.7	24.0
Core	0.693	0.421	4620	936	166.4	68.5
Bottom facesheet	0.148	0.174	987	387	12.6	16.1
<b>Case 2 {5, 5}</b>						
Top facesheet	0.324	0.225	2160	375	43.8	24.0
Core	1.281	0.513	8540	855	522.3	96.9
Bottom facesheet	0.133	0.165	889	275	10.8	14.8
<b>Case 3 {7, 7}</b>						
Top facesheet	0.317	0.229	2113	305	42.2	24.7
Core	1.161	0.496	7740	661	433.6	91.3
Bottom facesheet	0.133	0.164	887	219	10.7	14.7

wich plate. For each sandwich plate, the core will fail first, followed by the top facesheet and finally the bottom facesheet.

We have also calculated the approximate values of the maximum strain rate in each sandwich plate (column 4 and 5 of Table 10) by dividing the maximum plastic strain by the time taken to attain this value. The Miura-ori core deforms plastically at a much higher strain-rate ( $\sim 10^4 s^{-1}$ ) than the honeycomb core ( $\sim 10^3 s^{-1}$ ) indicating the level of strain rate for which material data is needed. Further, under the assumptions that the deformation process is adiabatic and that the entire plastic energy dissipated is converted to heat without any fraction being stored in the material microstructure, we have also estimated the maximum local temperature rise,  $\Delta T_r$  in each component of the sandwich plate (column 4 of Table 10) as  $\Delta T_r = ((\sigma_y + E_t \epsilon_p) \epsilon_p) / (2 \rho_m c)$ , where  $\sigma_y = 300$  MPa is the yield stress of the material,  $E_t = 2$  GPa is the hardening tangent modulus,  $\epsilon_p$  is the maximum equivalent plastic strain,  $\rho_m = 7800$  kg m<sup>-3</sup> is the material density and  $c = 450$  J/kg-K is the specific heat of the material. Clearly, the maximum local temperature rise at the end of the deformation process is larger in the Miura-ori core than that in the honeycomb core

**Table 11**

Magnitude of the peak overall reaction forces in the Miura-ori and the honeycomb-core sandwich plates for  $H = 10$  mm.

	Reaction force (kN)	
	Miura	HC
<b>Case 1 {3, 3}</b>		
Top facesheet	260.7	137.6
Bottom facesheet	104.8	110.8
<b>Case 2 {5, 5}</b>		
Top facesheet	186.1	141.2
Bottom facesheet	73.7	120.7
<b>Case 3 {7, 7}</b>		
Top facesheet	186.3	150.9
Bottom facesheet	75.6	119.5

suggesting that effects of thermal softening and thermal stresses may play important roles in these cores.

Finally, for  $P_0 = 100$  MPa, the magnitudes of the peak overall reaction forces along the edges of the top and the bottom facesheets are listed in Table 11 for the Miura-ori and the honeycomb core geometries detailed in Table 6. For the Miura-ori core, the reaction forces at the longitudinal edges of the facesheets ( $x = 0$  and  $x = 100$  mm) are unequal due to the asymmetry of the core and only the critical values are provided, while for the symmetric honeycomb core, all four edges of the facesheets have almost the same reaction force. The top facesheets of the Miura-ori core sandwich plates experience greater reaction forces than the corresponding honeycomb sandwich plates and hence need to be designed carefully, while the reaction forces experienced by bottom facesheets of the Miura-ori core sandwich plates are much less than that of the honeycomb sandwich plates again indicating the greater structural integrity offered by the Miura-ori core.

## 7. Conclusions

The response of Miura-ori core sandwich plates subject to blast loads has been analyzed by using the finite element commercial package ABAQUS/Explicit. Material strain rate effects and a failure criterion have not been considered in the analysis and it is assumed that the bonding between the core and the faces is perfect. Effects of the inertia forces developed in the core on its strengthening are illustrated through dynamic crushing simulations on the Miura-ori core at various loading rates. By comparing the performance of the four-node linear shell elements (element type S4R) with that of the three-dimensional eight-node brick elements (element type C3D8R) in capturing the crushing and buckling deformation patterns observed in the facets of the core as well as the elastic wave speeds in the core, it was shown that the S4R shell elements possess the requisite accuracy to model high-intensity dynamic deformations of foldcore sandwich plates. Following a discussion on the key phases of the mechanical response of the Miura-ori core architecture, we have delineated the influence of the unit cell parameters of the Miura-ori pattern on the response of the core and

compared its performance with that of the square honeycomb cores of equal areal density. Results clearly indicate that the Miura-ori cores consistently outperform honeycomb cores in terms of the energy dissipated through plastic deformations, particularly for moderate blast intensities. Furthermore, the Miura-ori core can achieve a wide range of sandwich behaviors by altering its unit cell parameters and hence offers a rich design space for tailoring its response to meet specified structural requirements.

## Acknowledgments

RCB's work was partially supported by the US Office of Naval Research grant N00014-16-1-2309 to Virginia Polytechnic Institute and State University with Dr. Y.D.S. Rajapakse as the program manager. Views expressed in the paper are those of the authors and neither of ONR nor of Virginia Tech.

## References

- [1] L.J. Gibson, M.F. Ashby, *Cellular Solids: Structure and Properties*, Cambridge university press, Cambridge, UK, 1999.
- [2] N. Fleck, V. Deshpande, The resistance of clamped sandwich beams to shock loading, *J. Appl. Mech.* 71 (3) (2004) 386–401.
- [3] V. Deshpande, N. Fleck, One-dimensional response of sandwich plates to underwater shock loading, *J. Mech. Phys. Solids* 53 (11) (2005) 2347–2383.
- [4] D. Radford, G. McShane, V. Deshpande, N. Fleck, The response of clamped sandwich plates with metallic foam cores to simulated blast loading, *Int. J. Solids Struct.* 43 (7) (2006) 2243–2259.
- [5] M. Tilbrook, V. Deshpande, N. Fleck, The impulsive response of sandwich beams: analytical and numerical investigation of regimes of behaviour, *J. Mech. Phys. Solids* 54 (11) (2006) 2242–2280.
- [6] J.W. Hutchinson, Z. Xue, Metal sandwich plates optimized for pressure impulses, *Int. J. Mech. Sci.* 47 (4) (2005) 545–569.
- [7] Z. Xue, J.W. Hutchinson, Crush dynamics of square honeycomb sandwich cores, *Int. J. Numer. Methods Eng.* 65 (13) (2006) 2221–2245.
- [8] Z. Xue, J.W. Hutchinson, A comparative study of impulse-resistant metal sandwich plates, *Int. J. Impact Eng.* 30 (10) (2004) 1283–1305.
- [9] G. McShane, V. Deshpande, N. Fleck, The underwater blast resistance of metallic sandwich beams with prismatic lattice cores, *J. Appl. Mech.* 74 (2) (2007) 352–364.
- [10] K.P. Dharmasena, H.N. Wadley, Z. Xue, J.W. Hutchinson, Mechanical response of metallic honeycomb sandwich panel structures to high-intensity dynamic loading, *Int. J. Impact Eng.* 35 (9) (2008) 1063–1074.
- [11] F. Zhu, L. Zhao, G. Lu, Z. Wang, Deformation and failure of blast-loaded metallic sandwich panels- experimental investigations, *Int. J. Impact Eng.* 35 (8) (2008) 937–951.
- [12] D. Karagiozova, G. Nurick, G. Langdon, S.C.K. Yuen, Y. Chi, S. Bartle, Response of flexible sandwich-type panels to blast loading, *Compos. Sci. Technol.* 69 (6) (2009) 754–763.
- [13] G. Nurick, G. Langdon, Y. Chi, N. Jacob, Behaviour of sandwich panels subjected to intense air blast-part 1: experiments, *Compos. Struct.* 91 (4) (2009) 433–441.
- [14] H. Rathbun, D. Radford, Z. Xue, M. He, J. Yang, V. Deshpande, N. Fleck, J. Hutchinson, F. Zok, A. Evans, Performance of metallic honeycomb-core sandwich beams under shock loading, *Int. J. Solids Struct.* 43 (6) (2006) 1746–1763.
- [15] S. Heims, P. Middendorf, S. Kilchert, A.F. Johnson, M. Maier, Experimental and numerical analysis of composite folded sandwich core structures under compression, *Appl. Compos. Mater.* 14 (5–6) (2007) 363–377.
- [16] S. Heims, Foldcore sandwich structures and their impact behaviour: an overview, in: *Dynamic failure of composite and sandwich structures*, Springer, 2013, pp. 491–544.
- [17] A. Lebé, K. Sab, Transverse shear stiffness of a chevron folded core used in sandwich construction, *Int. J. Solids Struct.* 47 (18) (2010) 2620–2629.
- [18] J. Gattas, Z. You, Quasi-static impact of indented foldcores, *Int. J. Impact Eng.* 73 (2014) 15–29.
- [19] J. Gattas, Z. You, The behaviour of curved-crease foldcores under low-velocity impact loads, *Int. J. Solids Struct.* 53 (2015) 80–91.
- [20] R. Fathers, J. Gattas, Z. You, Quasi-static crushing of eggbox, cube, and modified cube foldcore sandwich structures, *Int. J. Mech. Sci.* 101 (2015) 421–428.
- [21] M. Schenk, S.D. Guest, Geometry of Miura-folded metamaterials, *Proc. Natl. Acad. Sci.* 110 (9) (2013) 3276–3281.
- [22] C. Lv, D. Krishnaraju, G. Konjevod, H. Yu, H. Jiang, Origami based mechanical metamaterials, *Scientific reports* 4.
- [23] H. Yasuda, C. Chong, E.G. Charalampidis, P.G. Kevrekidis, J. Yang, Formation of rarefaction waves in origami-based metamaterials, *Phys. Rev. E* 93 (4) (2016) 043004.
- [24] T. Tachi, Generalization of rigid foldable quadrilateral mesh origami, in: *Symposium of the International Association for Shell and Spatial Structures (50th. 2009. Valencia). Evolution and Trends in Design, Analysis and Construction of Shell and Spatial Structures: Proceedings*, Editorial Universitat Politècnica de València, 2009.
- [25] T.A. Evans, R.J. Lang, S.P. Magleby, L.L. Howell, Rigidly foldable origami twists, *Origami6: I. Math.* (2015) 119.
- [26] X. Zhou, H. Wang, Z. You, Mechanical properties of Miura-based folded cores under quasi-static loads, *Thin-Walled Struct.* 82 (2014) 296–310.
- [27] S. Liu, G. Lu, Y. Chen, Y.W. Leong, Deformation of the Miura-ori patterned sheet, *Int. J. Mech. Sci.* 99 (2015) 130–142.
- [28] M. Schenk, S. Guest, G. McShane, Novel stacked folded cores for blast-resistant sandwich beams, *Int. J. Solids Struct.* 51 (25) (2014) 4196–4214.
- [29] R. Batra, T. Geng, Enhancement of the dynamic buckling load for a plate by using piezoceramic actuators, *Smart Mater. Struct.* 10 (5) (2001) 925.
- [30] R. Batra, N. Hassan, Response of fiber reinforced composites to underwater explosive loads, *Compos. Part B: Eng.* 38 (4) (2007) 448–468.
- [31] H. Türkmen, Z. Mecitoğlu, Dynamic response of a stiffened laminated composite plate subjected to blast load, *J. Sound Vib.* 221 (3) (1999) 371–389.
- [32] M. Alkhader, L. Bodelot, Large strain mechanical behavior of HSLA-100 steel over a wide range of strain rates, *J. Eng. Mater. Technol.* 134 (1) (2012) 011005.
- [33] R.C. Batra, N.M. Hassan, Blast Resistance of Unidirectional Fiber Reinforced Composites, *Compos. B* 39 (2008) 513–536.
- [34] R.C. Batra, R.N. Dubey, Impulsive Loading of Circular Plates, *Int. J. Solids Struct.* 7 (1971) 965–978.